Electrical Properties and Magnetic Response of Cobalt Germanosilicide Nanowires

Chun-I Tsai,[†,§] Chiu-Yen Wang,[†,§] Jianshi Tang,[‡] Min-Hsiu Hung,[†] Kang L. Wang,[‡] and Lih-Juann Chen[†,*]

[†]Department of Materials Science and Engineering, National Tsing Hua University, Hsinchu, Taiwan, 30013, Republic of China, and [‡]Device Research Laboratory, Department of Electrical Engineering, University of California, Los Angeles, California 90095, United States. [§]Authors with equal contribution.

ABSTRACT

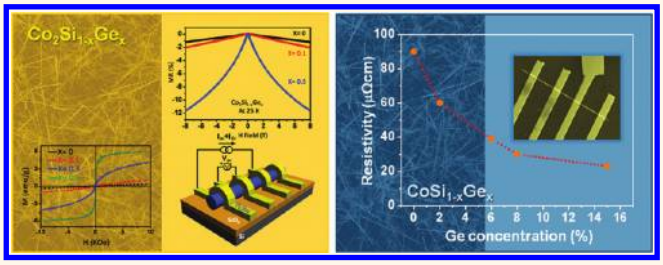

The effects of partial substitution of Ge for Si in cobalt germanosilicide ($CoSi_{1-x}Ge_x$ and $Co_2Si_{1-x}Ge_x$) nanowires (NWs) on the electrical transport, magnetic properties, and magnetoresistance (MR) have been investigated. Cobalt germanosilicide NWs were synthesized by a spontaneous chemical vapor transport growth method. The Ge concentration can be selectively controlled from 0 to 15% and 0−50% for $CoSi_{1-x}Ge_x$ and $Co_2Si_{1-x}Ge_x$ NWs, respectively, by varying the reaction temperature. Electrical measurements showed that the resistivities of $CoSi_{1-x}Ge_x$ NWs are 90, 60, 30, and 23 $\mu\Omega$-cm for $x = 0$, 0.01, 0.05, and 0.15, respectively. Therefore, the electrical resistivity of $CoSi_{1-x}Ge_x$ NWs was found to decrease significantly with an increasing Ge concentration, which is believed to be a result of the band gap narrowing. On the other hand, the $Co_2Si_{1-x}Ge_x$ ($x \leq 0.5$) NWs exhibited ferromagnetism at 300 K, which is attributed to the uncoordinated Co atoms on the NW surface and spin-glass behavior at low temperature. The highest MR response of $Co_2Si_{1-x}Ge_x$ NWs occurred at $x = 0.5$, where a MR ratio of 11.7% can be obtained at 10−25 K with a magnetic field of 8 T. The enhanced physical properties of cobalt germanosilicide NWs with Ge substitution shall lead to promising application in the fabrication of nanodevices, including spintronics and serving as the gate and interconnect material.

KEYWORDS: cobalt germanosilicide · nanowires · electrical transport · magnetoresistance · spintronics

Recently, increasing studies have been conducted on semiconductor alloy nanostructures because of their tunable band gap for device applications.[1−4] Among those semiconductor alloys, SiGe is of both scientific and technological importance. The SiGe alloys have a broad range of applications in fabricating heterojunction bipolar transistors, field-effect transistors, and optoelectronic silicon-based devices.[5−8] For those device applications, it is crucial to develop a good ohmic contact in nanoscale SiGe devices.

In the fabrication of ultra-large-scale integrated circuits, cobalt silicides have served essential roles in the gates and interconnect materials due to the low electrical resistivity and the compatibility of the silicidation process with current integrated circuit technology. Furthermore, CoSi alloys have a pseudogap at the Fermi level in an equilibrium structure, which can be reduced by Ge substitution, as reported by Kuo *et al.*[9] A significant decrease in the electrical resistivity was found in CoSi alloys as Si is partially replaced by Ge. As a result, single-crystalline cobalt germanosilicide nanowires (NWs) are regarded as a promising candidate for important applications in SiGe-based devices. In the literature, one-dimensional metal silicide nanostructures have been extensively investigated in the past decade.[10−28] The studies on the metal germanide nanostructures were also reported widely;[29−37] however, there are scarce reports on the synthesis and characterization of metal germanosilicide nanostructures.[38]

The magnetic properties of transition metal silicides in one-dimensional nanostructures have attracted considerable interest due to their interesting phenomena in the nanometer regime. For instance, room-temperature ferromagnetism in β-$FeSi_2$ and Fe_5Si_3 NWs as well as a high Curie temperature in Heusler alloy Fe_3Si NWs has been reported.[11−13] The signature of helimagnetic ordering in MnSi NWs was revealed *via* the magnetotransport study.[14−16] Ternary $Fe_{1-x}Co_xSi$ alloyed NWs displayed diverse magnetic behaviors including ferromagnetic semiconductor and helical magnet effects with different Co concentrations.[39,40] Bulk CoSi is a diamagnetic material; however, CoSi

* Address correspondence to ljchen@mx.nthu.edu.tw.

Received for review July 18, 2011 and accepted October 27, 2011.

Published online November 08, 2011
10.1021/nn202695a

NWs were discovered to exhibit a unique ferromagnetism at room temperature due to the presence of Co atoms with low coordination numbers on the surface.[17] Amorphous Co_2Ge exhibits a transition from paramagnetic state to spin-glass state at 41 K.[41] It could be suggested that the homogeneously mixed alloy of ternary cobalt germanosilicide ($CoSi_{1-x}Ge_x$ and $Co_2Si_{1-x}Ge_x$) NWs may display peculiar magnetic characteristics and improve the electrical properties.

In our previous work,[20] the composition of cobalt silicide nanostructures has been found to correlate with the reaction conditions. CoSi NWs can be obtained by a spontaneous chemical vapor transport (CVT) growth method with a growth temperature under 830 °C. Increasing the temperature to 880 °C can result in the formation of Co_2Si NWs. In this paper, we further developed a synthetic process to achieve the production of the cobalt germanosilicide NWs, including $CoSi_{1-x}Ge_x$ and $Co_2Si_{1-x}Ge_x$ phases, for the first time. In distinct growth temperature ranges, the Ge content in the cobalt germanosilicide NWs could be selectively controlled by varying the reaction temperature. From the electrical characteristics, the $CoSi_{1-x}Ge_x$ NWs exhibit a low resistivity of 23 $\mu\Omega$-cm with $x = 0.15$. Magnetic response of $Co_2Si_{1-x}Ge_x$ NWs verifies that these NWs possess physically distinctive signatures from both Co_2Si and $Co_2Si_{1-x}Ge_x$ ($x \leq 0.5$ in our study), which leads to a significant increase in the magnetoresistance (MR) ratio.

RESULTS AND DISCUSSION

Cobalt germanosilicide NWs were synthesized in the same furnace at various reaction temperatures by the spontaneous CVT method. The scheme of the detailed setup for the synthesis of cobalt germanosilicide NWs is depicted in the Supporting Information S1. The morphologies and elemental compositions of the NWs synthesized on the sample in region A were examined by scanning electron microscopy (SEM) and transmission electron microscopy (TEM), as shown in Figure 1. The SEM image reveals a high density of NWs of tens of micrometers in length. The low-magnification TEM image shows a clean and smooth surface of 80−100 nm in diameter. No catalyst and no secondary growth were observed. A selected area electron diffraction (SAED) pattern of a typical NW is shown in Figure 1c. The diffraction spots in the SAED pattern can be ascribed to the cubic B20-type CoSi and demonstrate that the NW growth is along the [$\bar{1}$10] direction. The corresponding high-resolution TEM (HRTEM) image is shown in Figure 1d and reveals that the NW is single-crystalline and defect-free. The energy-dispersive X-ray spectrometry (EDS) study by TEM indicates that the Ge content of the individual $CoSi_{1-x}Ge_x$ NWs (x = [Ge]/[Si] + [Ge]) is an average with a value of $x = 0.15 \pm 0.01$, as shown in Supporting Information S2(a).

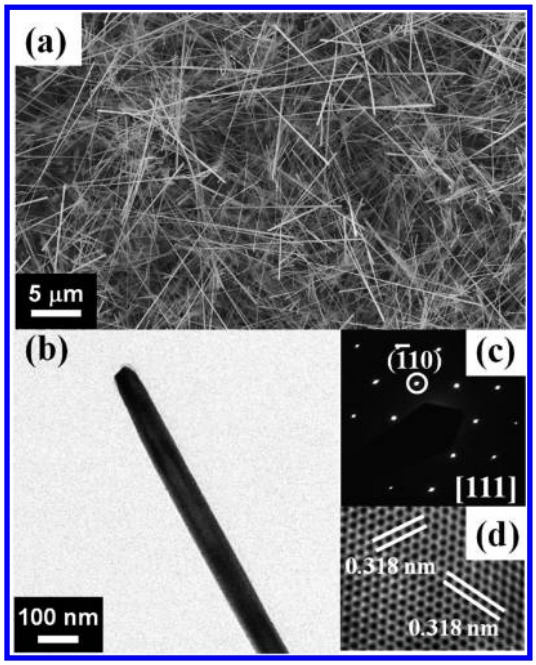

Figure 1. Structural characterization of $CoSi_{1-x}Ge_x$ NWs grown in region A. (a) Typical SEM image of $CoSi_{1-x}Ge_x$ NWs. (b) TEM image of a $CoSi_{1-x}Ge_x$ NW. (c) SAED pattern of a $CoSi_{1-x}Ge_x$ NW with the zone axis of [111]. (d) HRTEM image of a $CoSi_{1-x}Ge_x$ NW. The marked spacings of 0.318 nm correspond to both [$\bar{1}$10] and [$\bar{1}$01] planes.

The average value was obtained from the EDS measurements of about 10 NWs. The Ge element was homogeneously distributed in the whole NWs from the analysis of EDS spectra obtained at different locations of the NWs. The Ge content in the $CoSi_{1-x}Ge_x$ NWs could be controlled selectively by adjusting the reaction temperature of NW growth for $x = 0$, 0.01 ± 0.005, 0.05 ± 0.01, and 0.15 ± 0.01. The exact reaction temperatures measured with a thermocouple are 750, 770, 790, and 850 °C for $x = 0$, 0.01 ± 0.005, 0.05 ± 0.01, and 0.15 ± 0.01, respectively. All of them exhibit a similar morphology to that of $CoSi_{0.85}Ge_{0.15}$ NWs.

The Ge concentration of $CoSi_{1-x}Ge_x$ NWs was found to increase with the reaction temperature. This is the first report on the synthesis of cobalt germanosilicide NWs, even though the growth of many metal silicide NWs using metal halide precursors has been reported.[10−14,17,20,21] Vapor−solid mechanisms and self-catalyst growth are usually proposed in the growth process utilizing this method.[42] In a previous study on a ternary compound of $CoSi_{1-x}Ge_x$, the heat of formation was approximated from the relative crystal energies between CoSi and CoGe structures by a first-order approximation. It is suggested that the crystal energy of $CoSi_{1-x}Ge_x$ alloys would increase if Si atoms are partially replaced by Ge atoms.[43] The elevated reaction temperature could provide higher nucleation energy for $CoSi_{1-x}Ge_x$ NWs, which is needed for maintaining a stable compound with higher Ge content.

The substrate in the region B was positioned at a comparatively high temperature zone (880 °C). The

diameters and lengths of the NWs produced in this region are 80−100 nm and tens of micrometers, respectively, as illustrated in Figure 2a. The TEM image, SAED pattern, and HRTEM image of a NW are shown in Figure 2b, c, and d, respectively. The SAED pattern can be identified as an orthorhombic Co_2Si structure, and the regular spot pattern of the electron diffraction confirmed the single-crystalline nature of NWs. The result is consistent with the HRTEM image shown in Figure 2d. The TEM-EDS study in Supporting Information S2(b) indicates that the Ge content of the individual $Co_2Si_{1-x}Ge_x$ NWs has an average value of $x = 0.5 \pm 0.03$. The average value was obtained from the EDS spectra of about 10 NWs. The Ge element was homogeneously distributed over the whole NWs from the analysis of the EDS spectra obtained from different places of the NWs. The $Co_2Si_{1-x}Ge_x$ NWs could be synthesized with a controlled Ge concentration by varying reaction temperature. The Ge concentrations (x) and temperature are 0, 0.1 ± 0.01, 0.5 ± 0.03 and 880, 900, and 950 °C, respectively. All have a similar morphology to the $Co_2Si_{0.5}Ge_{0.5}$ NWs.

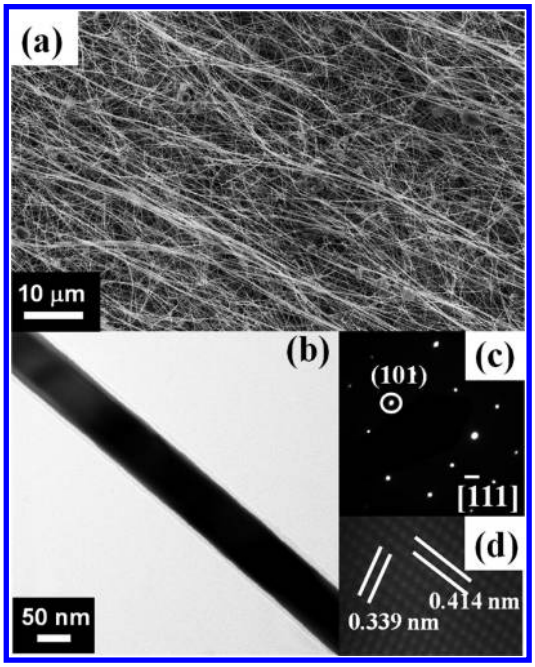

Figure 2. Structural characterization of $Co_2Si_{1-x}Ge_x$ NWs grown in region B. (a) Typical SEM image of $Co_2Si_{1-x}Ge_x$ NWs. (b) TEM image of a $Co_2Si_{1-x}Ge_x$ NW. (c) SAED pattern of a $Co_2Si_{1-x}Ge_x$ NW with the zone axis of [$\bar{1}$11]. (d) HRTEM image of a $Co_2Si_{1-x}Ge_x$ NW. The marked spacings of 0.414 and 0.339 nm correspond to the [01$\bar{1}$] and [101] planes, respectively.

The X-ray powder diffraction (XRD) measurements on the $Co_2Si_{1-x}Ge_x$ NWs samples were also performed for phase identification. The XRD patterns of $Co_2Si_{1-x}Ge_x$ NWs are displayed in Figure 3a, which indicate that all peaks can be ascribed to the Co_2Si phase (JCPDS file: 89-4181). The peaks due to any other traceable impurity phase were not observed. With the increase of Ge concentration, it was found that the peaks shift to lower angles and the widths of peaks become broader. To scrutinize the peak shift, the $\Delta(2\theta)$ in the (002) plane is 0.22° and 0.63° for $x = 0.1$ and 0.5, respectively. The variation of the lattice parameter as a function of Ge concentration is shown in Figure 3b. It is clearly seen that the lattice constant increases with Ge content, indicating that the Si sites are partially substituted by Ge atoms, according to Vegard's law. The XRD data of $CoSi_{1-x}Ge_x$ NWs are not shown. Because of the large peak widths, the concentration of Ge in the NWs could not be readily determined by the shift of the peak position.

Electrical transport properties of cobalt germanosilicide NWs with various Ge content have been measured by the four-terminal $I-V$ method. The SEM image of a typical NW device is shown in the inset of Figure 4. The resistivity values were obtained from 4 to 5 NWs for each Ge concentration. The average resistivities and Ge contents of the $CoSi_{1-x}Ge_x$ NWs are 90, 60, 30, and 23 $\mu\Omega$-cm for $x = 0$, 0.01, 0.05, and 0.15, respectively, as illustrated in Figure 4. The detailed $I-V$ curves of individual $CoSi_{1-x}Ge_x$ NWs are shown in Supporting Information S3(a). The values match well with the reported value of CoSi NWs (126 $\mu\Omega$-cm)[17] and approach that reported for bulk single-crystalline $CoSi_2$ (18 $\mu\Omega$-cm),[44] which is the lowest resistivity for cobalt silicides. A decrease in resistivity was observed with the increase in Ge content of $CoSi_{1-x}Ge_x$ NWs. A previous

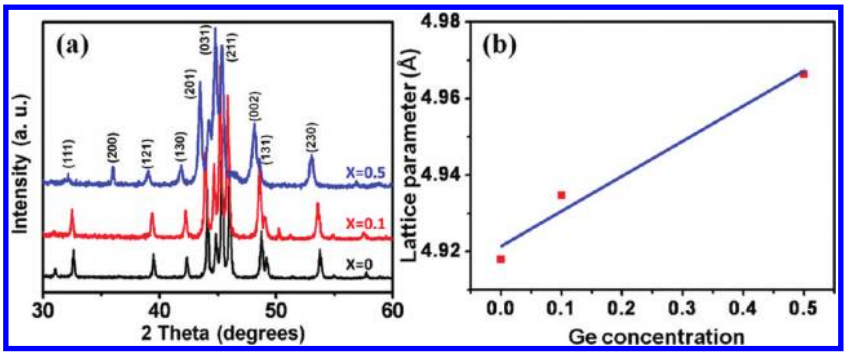

Figure 3. (a) XRD patterns of the $Co_2Si_{1-x}Ge_x$ NWs with $x = 0$, 0.1, and 0.5. (b) Lattice parameter *versus* Ge concentration as obtained from XRD.

study on the bulk $CoSi_{1-x}Ge_x$ has revealed the semimetallic characteristics of this compound, and the semimetallic nature is associated with the low density of states (DOS) at the Fermi level.[9] The Ge substitution for Si could narrow the band gap due to an increase of the DOS at the Fermi level. The reduction in the electrical resistivity with the increase in Ge content would correspond to the decrease of the band gap. The electrical transport measurements of $Co_2Si_{1-x}Ge_x$ NWs have been characterized, and the detailed data are shown in Supporting Information S3(b). The resistivities and Ge contents of the $Co_2Si_{1-x}Ge_x$ NWs are 180, 187, and 102 $\mu\Omega$-cm for $x = 0$, 0.1, and 0.5, respectively, which match well with the value reported for single-crystalline Co_2Si NWs (200 $\mu\Omega$-cm).[21]

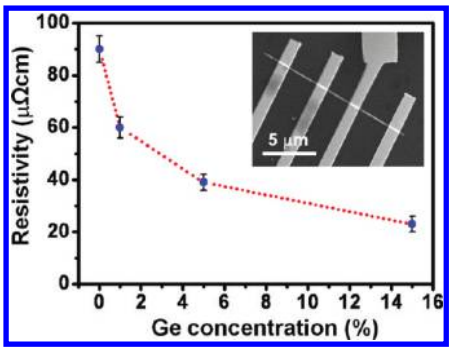

Figure 4. Resistivity *versus* Ge content curves of $CoSi_{1-x}Ge_x$ NWs. The resistivity of a NW decreases with increasing Ge concentration. The inset is a typical SEM image of the electrical device fabricated with the standard EBL processes.

In situ annealing TEM was used to investigate the thermal stability property of $CoSi_{1-x}Ge_x$ NWs in real time. The samples were produced by scraping the as-grown NW samples on a TEM Mo grid (with carbon film windows). As seen in Supporting Information S4, the TEM images reveal that the morphology of the $CoSi_{0.85}Ge_{0.15}$ NW remained intact as the temperature was ramped to 950 °C (100 °C min^{-1}) and then held for 30 min. The structural information and composition of the annealed $CoSi_{0.85}Ge_{0.15}$ NWs were obtained from TEM analyses (Supporting Information S4). A SAED pattern obtained from an annealed NW shows regular spots, indicating the single-crystalline nature and can be indexed to the cubic CoSi structure. From the EDS spectrum (not shown), the ratio of Co:Si:Ge is approximately 1:0.85:0.15. The TEM analyses of SAED pattern and EDS spectra of several annealed NWs show the same structure and chemical composition as the

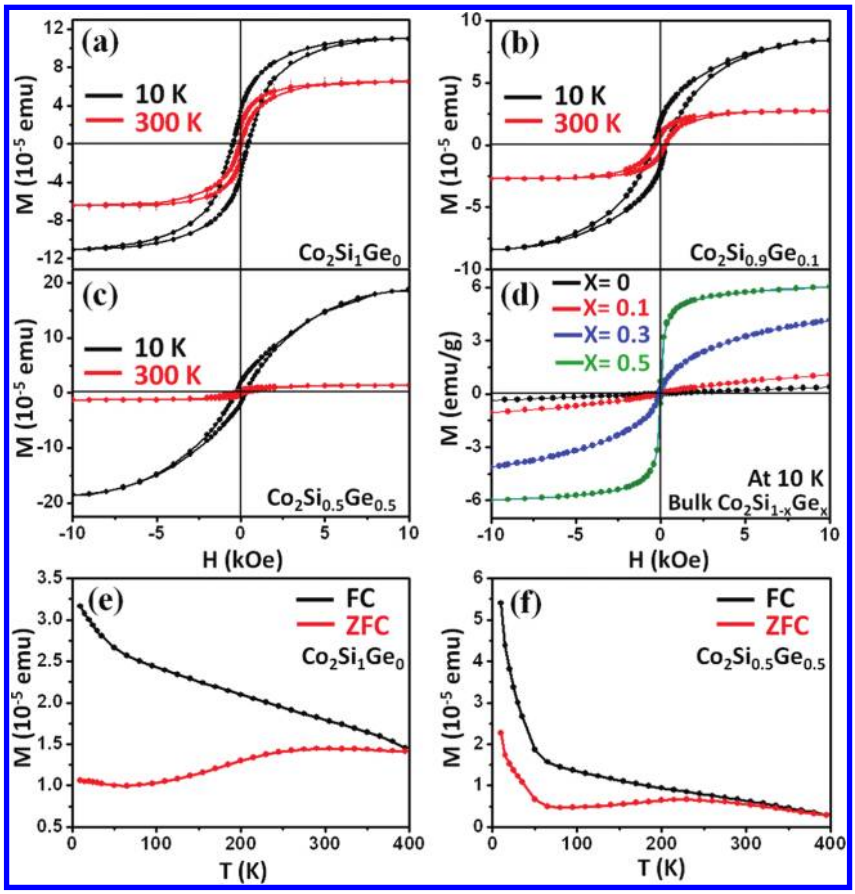

Figure 5. (a–c) Plot of the magnetization, *M*, as a function of the magnetic field, *H*, obtained from the $Co_2Si_{1-x}Ge_x$ NWs with $x = 0$, 0.1, and 0.5, respectively, at 10 and 300 K. (d) Plot of the *M*–*H* curves obtained from the bulk $Co_2Si_{1-x}Ge_x$ alloys with various Ge concentrations ($x = 0$, 0.1, 0.3, and 0.5) at 10 K. (e and f) Plot of *M* as a function of *T* at an applied field of 100 Oe obtained from $Co_2Si_{1-x}Ge_x$ NWs with $x = 0$ and 0.5, respectively. Black and red lines represent the field-cooling (FC) and zero-field-cooling (ZFC) data, respectively.

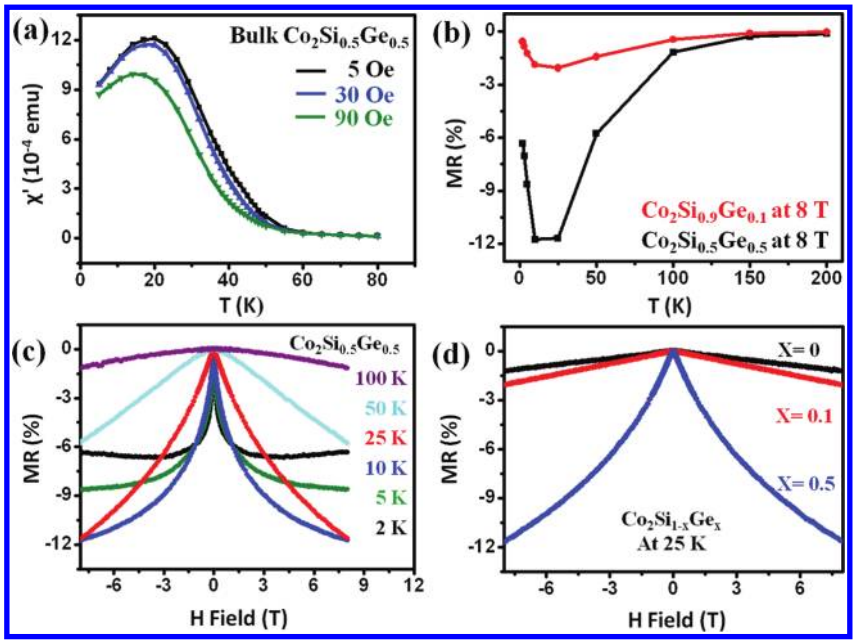

Figure 6. (a) Temperature dependence at 109 Hz of the AC susceptibility of bulk $Co_2Si_{0.5}Ge_{0.5}$ under different applied magnetic fields. (b) Temperature dependence MR of $Co_2Si_{1-x}Ge_x$ (x = 0.1 and 0.5) NWs. (c) Magnetotransport measurements of an individual $Co_2Si_{0.5}Ge_{0.5}$ NW with an applied field (up to 8 T) at various temperatures. (d) MR measurements of $Co_2Si_{1-x}Ge_x$ NWs with x = 0, 0.1, and 0.5 at 25 K.

unannealed NWs, indicating that the $CoSi_{1-x}Ge_x$ NWs have a high thermal stability.

The magnetic properties of $Co_2Si_{1-x}Ge_x$ NWs were measured with the superconducting quantum interference device (SQUID) magnetometer. Figure 5a–c show plots of the magnetization *versus* the applied magnetic field (*M versus H*) at temperatures of 10 and 300 K for the NWs with x = 0, 0.1, and 0.5. A ferromagnetism signature at room temperature was observed from the hysteresis loops with nonzero remnant magnetization and coercivity for the $Co_2Si_{1-x}Ge_x$ NWs. The ferromagnetic behaviors in the NWs are attributed to the reduced coordination of the Co atoms on the $Co_2Si_{1-x}Ge_x$ NWs surface,[17] considering that the NW surface to volume ratio is high. The magnetic moment per surface Co atom of $Co_2Si_{1-x}Ge_x$ NWs from the M–H data was estimated, as shown in Supporting Information S5. The variation in the NW diameters (80–100 nm) has been taken into consideration by averaging the fraction of Co atoms at the surface. The calculated average magnetic moments per surface Co atom of $Co_2Si_{1-x}Ge_x$ NWs are 1.53, 1.20, and 1.85 for x = 0, 0.1, and 0.5, respectively. The values are in general agreement with the reported magnetic moment of the Co atom of 1.72 μ_B.[17]

For the M–H curves of $Co_2Si_{1-x}Ge_x$ NWs, the divergences of saturated magnetization at 10 and 300 K became larger with increasing Ge content. For comparison, alloys with the same composition of $Co_2Si_{1-x}Ge_x$ NWs were prepared using an arc melting furnace in a water-cooled copper crucible under Ar atmosphere. The M–H curves of bulk $Co_2Si_{1-x}Ge_x$ samples were obtained, and a similar magnetic signature was also observed, as illustrated in Figure 5d. The saturation of the magnetization close to H = 0 becomes more abrupt with increasing Ge concentration. The features in the magnetic response resemble closely the spin-glass-like behavior, due to a spin disorder system (frustrated interaction) augmented by the stochastic disorder. In a previous study, the spin-glass behavior of bulk amorphous Co_2Ge was reported.[41] This material exhibits a single transition from paramagnetic to the spin-glass state at 41 K (T_f, freezing temperature). The temperature dependences of magnetization for $Co_2Si_1Ge_0$ NWs and $Co_2Si_{0.5}Ge_{0.5}$ NWs have been measured during zero-field-cooling (ZFC) and field-cooling (FC) under an applied field of 100 Oe, as shown in Figure 5e and f, respectively. The ZFC and FC curves of $Co_2Si_{0.5}Ge_{0.5}$ NWs show a steep decrease at temperatures below 50 K. However, these features are not observed in the FC or ZFC curves of $Co_2Si_1Ge_0$ NWs.

AC magnetization measurements of bulk $Co_2Si_{0.5}Ge_{0.5}$ were performed at a frequency of 109 Hz under different magnetic fields of 5, 30, and 90 Oe. Figure 6a shows that the freezing temperature (T_f) of bulk $Co_2Si_{0.5}Ge_{0.5}$ is shifted to lower temperature and the intensity of susceptibility (χ') is decreased with increasing magnetic field (5, 30, and 90 Oe) at 109 Hz. The results are similar to spin-glass behavior of amorphous Co_2Ge that was reported by Zhou *et al.*[41] However, the freezing temperature of amorphous Co_2Ge (T_f is 41 K) is higher than our single-crystalline $Co_2Si_{1-x}Ge_x$ system (T_f ~25 K). The interaction of the crystalline $Co_2Si_{1-x}Ge_x$ ternary system needs more detailed magnetic property study. MR measurements for individual

$Co_2Si_{1-x}Ge_x$ NWs were carried out with an applied magnetic field. To prepare a MR device, the NWs were dispersed on a SiO_2/Si substrate and the 30/120 nm Cr/Au contacts to an individual NW were defined with electron beam lithography (EBL). Figure 6b is the temperature-dependent MR of $Co_2Si_{1-x}Ge_x$ NWs (x = 0.1 and 0.5), which also shows a maximum value at 10−25 K. The results were consistent with the ac magnetization measurements of bulk $Co_2Si_{0.5}Ge_{0.5}$ in Figure 6a. The MR *versus* applied magnetic field (up to 8 T) curves at temperatures of 100, 50, 25, 10, 5, and 2 K for $Co_2Si_{0.5}Ge_{0.5}$ NWs are plotted in Figure 6c. The MR curves at 5 and 2 K show a quick saturation as the applied field exceeds 2 T and a negative MR was observed at all temperatures. These MR features are similar to the reports of Co_2Si nanobelts.[19] Figure 6d shows the MR data of $Co_2Si_{1-x}Ge_x$ NWs with x = 0, 0.1, and 0.5 at 25 K. Maximum MR ratios of 1.21%, 2.07%, and 11.7% were observed with increasing Ge content (x = 0, 0.1, and 0.5, respectively) under the magnetic field of 8 T. Generally, MR effects in silicide nanostructure can be attributed to the interaction of conducting electrons with spins of localized dangling bonds. The Si was substituted by Ge in $Co_2Si_{1-x}Ge_x$ NWs, as mentioned above, and could augment the stochastic disorder spin due to the spin-glass behavior from the $Co_2Si_{1-x}Ge_x$ ($x \leq 0.5$) compound. This may explain the relatively large MR values of $Co_2Si_{1-x}Ge_x$ NWs compared to those reported in a previous study for Co_2Si NWs.[20] The physical properties observed for $Co_2Si_{1-x}Ge_x$ NWs verify that these NWs possess physically distinctive features from Co_2Si and $Co_2Si_{1-x}Ge_x$ ($x \leq 0.5$). The measurements of magnetic properties for $CoSi_{1-x}Ge_x$ NWs have been carried out. As seen in Supporting Information S6, the room-temperature ferromagnetic properties were also observed in $CoSi_{1-x}Ge_x$ NWs, but the spin-glass behavior was not present in $CoSi_{1-x}Ge_x$ NWs with the Ge substitution. Therefore, almost no MR effect (the MR data are not shown) in $CoSi_{1-x}Ge_x$ NWs was observed. The room-temperature ferromagnetic behavior and the large MR response of $Co_2Si_{1-x}Ge_x$ NWs suggest that $Co_2Si_{1-x}Ge_x$ NWs have great potentials in versatile applications for Si/Ge-based spintronics.

SUMMARY AND CONCLUSIONS

In summary, cobalt germanosilicide ($CoSi_{1-x}Ge_x$ and $Co_2Si_{1-x}Ge_x$) NWs have been synthesized *via* a spontaneous CVT growth method in one step. The Ge concentration can be selectively controlled from 0 to 15% and 0−50% for $CoSi_{1-x}Ge_x$ and $Co_2Si_{1-x}Ge_x$ NWs, respectively, by varying the reaction temperature. The elemental components are uniformly distributed along the free-standing NWs. The resistivity of $CoSi_{1-x}Ge_x$ NWs was found to decrease with increasing Ge content, and the structure remained intact at high temperature (950 °C). The reduction in electrical resistivity with the increase in Ge content would correspond to the decrease in the magnitude of the band gap resulting from the Ge substitution with Si. The room-temperature ferromagnetism and the reentrant spin-glass-like behavior of $Co_2Si_{1-x}Ge_x$ NWs were discovered. The large MR performance of 11.7% at 10−25 K indicates that $Co_2Si_{1-x}Ge_x$ NWs have great potential in spintronics applications. The superior electrical characteristics and MR properties indicate that the cobalt germanosilicide NWs could play an important role in versatile applications for Si/Ge-based nanodevices.

EXPERIMENTAL SECTION

Single-crystalline Si(001) wafers were used as the substrate for the NW growth. Prior to loading into a two-zone furnace at the atmospheric pressure with argon (Ar) flow, the wafer was cleaned with 1%-buffered HF. The samples were placed downstream, with the cobalt chloride and germanium powders upstream. The powders were then heated at 600 °C, and the heating zone was set at temperatures of 750−1000 °C. The two heating centers were 20 cm apart. The temperature was ramped up from room temperature to the reaction temperature in 60 min. The exact temperature of the substrate was measured with a thermocouple attached to it. The precursor vapors were carried by the Ar flow of 100 sccm and reacted on the silicon substrates placed downstream for 2 h. The furnace was then cooled to room temperature. The NW product was investigated by XRD, and the morphology was examined with a field emission SEM (JSM-6500F). The phase and composition of nanostructures were obtained with a JEOL-2010 TEM, equipped with EDS. To prepare devices for the electrical measurements, as-synthesized NWs were transferred to a SiO_2/Si substrate, and EBL was used to define 30 nm/120 nm Cr/Au contacts on NWs. Before the deposition of electrodes, the sample was dipped into a dilute HF solution for 5 s to remove the native oxide in the contact region. Agilent B1500A semiconductor device analyzer with a four-probe station was used for electrical measurements. The magnetic properties of cobalt germanosilicide NWs were characterized using a SQUID magnetometer. For the magneto-transport properties of cobalt germanosilicide NWs, four-terminal Au wire bonded devices were measured at various temperatures and magnetic fields using a Quantum Design Physical Property Measurement System.

Acknowledgment. The authors acknowledge the support from National Science Council through grant no. NSC 98-2221-E-007-104-MY3. This work was in part supported by Western Institution of Nanoelectronics (WIN) and Focus Center on Functional Engineered Nano Architectonics (FENA).

Supporting Information Available: This material is available free of charge via the Internet at http://pubs.acs.org.

REFERENCES AND NOTES

1. Duan, X.; Huang, Y.; Cui, Y.; Wang, J.; Lieber, C. M. Indium Phosphide Nanowires as Building Blocks for Nanoscale Electronic and Optoelectronic Devices. *Nature* **2001**, *409*, 66–69.
2. Huang, C. T.; Song, J. H.; Lee, W. F.; Ding, Y.; Gao, Z. Y.; Hao, Y.; Chen, L. J.; Wang, Z. L. GaN Nanowire Arrays for High-Output Nanogenerators. *J. Am. Chem. Soc.* **2010**, *132*, 4766–4771.

3. Goldberger, J.; He, R.; Zhang, Y.; Lee, S.; Yan, H.; Choi, H. J.; Yang, P. Single-Crystal Gallium Nitride Nanotubes. *Nature* **2003**, *422*, 599–602.
4. Xiang, J.; Lu, W.; Hu, Y.; Wu, Y.; Yan., H.; Lieber, C. M. Ge/Si Nanowire Heterostructures as High-Performance Field-Effect Transistors. *Nature* **2006**, *441*, 489–493.
5. Wen, C. Y.; Reuter, M. C.; Bruley, J.; Tersoff, J.; Kodambaka, S.; Stach, E. A.; Ross, F. M. Formation of Compositionally Abrupt Axial Heterojunctions in Silicon-Germanium Nanowires. *Science* **2009**, *326*, 1247–1250.
6. Wu, Y.; Fan, R.; Yang, P. Block-by-Block Growth of Single-Crystalline Si/SiGe Superlattice Nanowires. *Nano Lett.* **2002**, *2*, 83–86.
7. Clark, T. E.; Nimmatoori, P.; Lew, K. K.; Pan, L.; Rewing, J. M.; Dickey, E. C. Diameter Dependent Growth Rate and Interface Abruptness in Vapor-Liquid-Solid Si/$Si_{1-x}Ge_x$ Heterostructure Nanowires. *Nano Lett.* **2008**, *8*, 1246–1252.
8. He, J. H.; Chen, C. Y.; Ho, C. H.; Wang, C. W.; Chen, M. J.; Chen, L. J. Growth and Structural Characterization of SiGe Nanorings. *J. Phys. Chem. C* **2010**, *114*, 5727–5731.
9. Kuo, Y. K.; Sivakumar, K. M.; Huang, S. J.; Lue, C. S. Thermoelectric Properties of the $CoSi_{1-x}Ge_x$ Alloys. *J. Appl. Phys.* **2005**, *98*, 123510.
10. Schmitt, A. L.; Higgins, J. M.; Szczech, J. R.; Jin, S. Synthesis and Applications of Metal Silicide Nanowires. *J. Mater. Chem.* **2010**, *20*, 223–235.
11. Seo, K.; Bagkar, N.; Kim, S.; In, J.; Yoon, H.; Jo, Y.; Kim, B. Diffusion-Driven Crystal Structure Transformation: Synthesis of Heusler Alloy Fe_3Si Nanowires. *Nano Lett.* **2010**, *10*, 3643–3647.
12. Hung, S. W.; Yeh, P. H.; Chu, L. W.; Chen, C. D.; Chou, L. J.; Wu, Y. J.; Chen, L. J. Direct Growth of β-$FeSi_2$ Nanowires with Infrared Emission, Ferromagnetism at Room Temperature and High Magnetoresistance *via* a Spontaneous Chemical Reaction Method. *J. Mater. Chem.* **2011**, *21*, 5704–5709.
13. Hung, S. W.; Wang, T. J.; Chu, L. W.; Chen, L J. Orientation-Dependent Room-Temperature Ferromagnetism of FeSi Nanowires and Applications in Nonvolatile Memory Devices. *J. Phys. Chem. C* **2011**, *115*, 15592–15597.
14. Seo, K.; Yoon, H.; Ryu, S. W.; Lee, S.; Jo, Y.; Jung, M. H.; Kim, J.; Choi, Y. K.; Kim, B. Itinerant Helimagnetic Single-Crystalline MnSi Nanowires. *ACS Nano* **2010**, *4*, 2569–2576.
15. Chang, M. T.; Chen, C. Y.; Chou, L. J.; Chen, L . J. Core-Shell Chromium Silicide−Silicon Nano-Pillars: Contact Material for Future Nano-Systems. *ACS Nano* **2019**, *3*, 3776–3780.
16. Higgins, J. M.; Ding, R.; DeGrave, J. P.; Jin, S. Signature of Helimagnetic Ordering in Single-Crystal MnSi Nanowires. *Nano Lett.* **2010**, *10*, 1605–1610.
17. Seo, K.; Varadwaj, K. S. K.; Mohanty, P.; Lee, S.; Jo, Y.; Jung, M. H.; Kim, J.; Kim, B. Magnetic Properties of Single-Crystalline CoSi Nanowires. *Nano Lett.* **2007**, *7*, 1240–1245.
18. Schmitt, A. L.; Zhu, L.; Schmeisser, D.; Himpsel, F. J.; Jin, S. Metallic Single-Crystal CoSi Nanowires *via* Chemical Vapor Deposition of Single-Source Precursor. *J. Phys. Chem. B* **2006**, *110*, 18142–18146.
19. Qu, Y.; Bai, J.; Liao, L.; Cheng, R.; Lin, Y. C.; Huang, Y.; Guo, T.; Duan, X. Synthesis and Electric Properties of Dicobalt Silicide Nanobelts. *Chem. Commun.* **2011**, *47*, 1255–1257.
20. Tsai, C. I.; Yeh, P. H.; Wang, C. Y.; Wu, H. W.; Chen, U. S.; Lu, M. Y.; Wu, W. W.; Chen, L. J.; Wang, Z. L. Cobalt Silicide Nanostructures: Synthesis, Electron Transport and Field Emission Properties. *Cryst. Growth Des.* **2009**, *9*, 4514–4518.
21. Seo, K.; Lee, S.; Yoon, H.; In, J.; Varadwaj, K. S. K.; Jo, Y.; Jung, M. H.; Kim, J; Kim, B. Composition-Tuned Co_nSi Nanowires: Location-Selective Simultaneous Growth along Temperature Gradient. *ACS Nano* **2009**, *3*, 1145–1150.
22. Zhou, F.; Szczech, J.; Pettes, M. T.; Moore, A. L.; Jin, S.; Shi, L. Determination of Transport Properties in Chromium Disilicide Nanowires *via* Combined Thermoelectric and Structural Characterizations. *Nano Lett.* **2007**, *7*, 1649–1654.
23. Chen, L. J. Metal Silicides: an Integral Part of Microelectronics. *JOM* **2005**, *57* (9), 24–30.
24. Song, Y.; Schmitt, A. L.; Jin, S. Ultralong Single-Crystal Metallic Ni_2Si Nanowires with Low Resistivity. *Nano Lett.* **2007**, *7*, 965–969.
25. Lee, C. Y.; Lu, M. P.; Liao, K. F.; Wu, W. W.; Chen, L. J. Vertically Well-Aligned Epitaxial $Ni_{31}Si_{12}$ Nanowire Arrays with Excellent Field Emission Properties. *Appl. Phys. Lett.* **2008**, *93*, 113109.
26. Lee, C. Y.; Lu, M. P.; Liao, K. F.; Lee, W. F.; Huang, C. T.; Chen, S. Y.; Chen, L. J. Free-Standing Single Crystal $NiSi_2$ Nanowires with Excellent Electrical Transport and Field Emission Properties. *J. Phys. Chem. C* **2009**, *113*, 2286–2289.
27. Chang, C. M.; Chang, Y. C.; Chung, Y. A.; Lee, C. Y.; Chen, L. J. Synthesis and Properties of the Low Resistivity $TiSi_2$ Nanowires Grown with TiF_4 Precursor. *J. Phys. Chem. C* **2009**, *113*, 17720–17723.
28. Chang, C. M.; Chang, Y. C.; Lee, C. Y.; Yeh, P. H.; Lee, W. F.; Chen, L. J. Synthesis and Physical Properties of Ti_5Si_4 Nanobats. *J. Phys. Chem. C* **2009**, *113*, 9153–9156.
29. Tang, J.; Wang, C. Y.; Xiu, F.; Hong, A. J.; Chen, S.; Wang, M.; Zeng, C.; Yang, H. J.; Tuan, H. Y.; Tsai, C. J.; Chen, L. J.; Wang, K. L. Single-Crystalline Ni_2Ge/Ge/Ni_2Ge Nanowire Heterostructure Transistors. *Nanotechnology* **2010**, *21*, 505704.
30. Tang, J.; Wang, C. Y.; Xiu, F.; Lang, M.; Chu, L. W.; Tsai, C. J.; Chueh, Y. L.; Chen, L. J.; Wang, K. L. Oxide-Confined Formation of Ge Nanowire Heterostructure for High Performance Transistors. *ACS Nano* **2011**, *5*, 6008–6015.
31. Tang, J.; Wang, C. Y.; Xiu, F.; Zhou, Y.; Chen, L. J.; Wang, K. L. Formation and Device Application of Ge Nanowire Heterostructures *via* Rapid Thermal Annealing. *Adv. Mater. Sci. Eng.* **2011**, *2011*, 316513.
32. Yoon, H.; Kang, T.; Lee, J. M.; Kim, S. I.; Seo, K.; Kim, J.; Park, W. I.; Kim, B. Epitaxially Integrating Ferromagnetic $Fe_{1.3}Ge$ Nanowire Arrays on Few-Layer Grapheme. *J. Phys. Chem. Lett.* **2011**, *2*, 956–960.
33. Yoon, H.; Lee, A. T.; Choi, E.; Seo, K.; Bagkar, N.; Cho, J.; Chang, K. J.; Kim, B. Structure-Induced Ferromagnetic Stabilization in Freestanding Hexagonal $Fe_{1.3}Ge$ NWs. *J. Am. Chem. Soc.* **2010**, *49*, 17447–17451.
34. Yoon, H.; Seo, K.; Bagkar, N.; In, J.; Park, J.; Kim, J.; Kim, B. Vertical Epitaxial Co_5Ge_7 Nanowire and Nanobelt Arrays on a Thin Graphitic Layer for Flexible Field Emission Display. *Adv. Mater.* **2009**, *21*, 4979–4982.
35. Dellas, N. S.; Minassian, S.; Redwing, J. M.; Mohney, S. E. Formation of Nickel Germanide Contacts to Ge Nanowires. *Appl. Phys. Lett.* **2010**, *97*, 263116.
36. Burchhart, T.; Lugstein, A.; Hyun, Y. J.; Hochleitner, G.; Bertagnolli, E. Atomic Scale Alignment of Copper-Germanide Contacts for Ge Nanowire Metal Oxide Field Effect Transistors. *Nano Lett.* **2009**, *9*, 3739–3742.
37. Yan, C.; Higgins, J. M.; Faber, M. S.; Lee, P. S.; Jin, S. Spontaneous Growth and Phase Transformation of Highly Conductive Nickel Germanide Nanowires. *ACS Nano* **2011**, *5*, 5006–5014.
38. Higgins, J. M.; Carmichael, P.; Schmitt, A. L.; Lee, S.; Degrave, J. P.; Jin, S. Mechanistic Investigation of the Growth of $Fe_{1-x}Co_xSi$ ($0 \le x \le 1$) and $Fe_5(Si_{1-y}Ge_y)_3$ ($0 \le y \le 0.33$) Ternary Alloy Nanowires. *ACS Nano* **2011**, *5*, 3268–3277.
39. Schmitt, A. L.; Higgins, J. M.; Jin, S. Chemical Synthesis and Magnetotransport of Magnetic Semiconducting of $Fe_{1-x}Co_xSi$ Alloy Nanowires. *Nano Lett.* **2008**, *8*, 810–815.
40. In, J.; Varadwaj, K. S. K.; Seo, K.; Lee, S.; Jo, Y.; Jung, M. H.; Kim, J.; Kim, B. Single-Crystalling Ferromagnetic $Fe_{1-x}Co_xSi$ Nanowires. *J. Phys. Chem. C* **2008**, *112*, 4748–4752.
41. Zhou, G. F.; Bakker, H. Spin-Glass Behavior of Amorphous Co_2Ge Synthesized by Mechanical Milling. *Phys. Rev. Lett.* **1994**, *72*, 2290–2293.
42. Ouyang, L.; Thrall, E. S.; Deshmukh, M. M.; Park, H. Vapor-Phase Synthesis and Characterization of ε-FeSi Nanowires. *Adv. Mater.* **2006**, *18*, 1437–1440.
43. Wang, Z.; Aldrich, D. B.; Chen, Y. L.; Sayers, D. E.; Nemanich, R. J. Silicide Formation and Stability of Ti/SiGe and Co/SiGe. *Thin Solid Films* **1995**, *270*, 555–560.
44. Lauwers, A.; Besser, P.; Gutt, T.; Satta, A.; Potter, M.; Lindsay, R.; Roelandts, N.; Loosen, F.; Jin, S.; Bender, H.; Stucchi, M.; Vrancken, C.; Deweerdt, B.; Maex, K. Comparative Study of Ni-Silicide and Co-Silicide for sub 0.25-μm Technologies. *Microelectron. Eng.* **2000**, *50*, 103–116.